Synthesis and Evaluation of Cellulose-based, 1,2,3-Triazolium-functionalized Polymerized Ionic Liquids: Thermal Transitions, Ionic Conductivities and Morphological Properties

Rose J. Miller,[1] Vanessa M. Smith,[1] Stacy A. Love,[2] Sarah M. Byron,[1] David Salas-de la Cruz,[2,3] Kevin M. Miller[1,*]

[1]Department of Chemistry, Murray State University, Murray, KY 42017.

[2]Center for Computational and Integrative Biology, Rutgers University, Camden, NJ, United States of America

[3]Department of Chemistry, Rutgers University, Camden, NJ, United States of America

*Corresponding Author: Kevin M. Miller, kmiller38@murraystate.edu

ABSTRACT:

A series of 1,2,3-triazolium-functionalized cellulose derivatives were prepared using an azide-alkyne 'click' cyclization strategy, followed by quaternization. As cellulose represents an inexpensive and sustainable biomacromolecule, the ability to functionalize the backbone with an ionic liquid and generate a new class of conductive materials is of great interest. Here, three different counteranions ([Br], [OTf] and [NTf_2]) were employed in order to explore the interplay between thermal, conductive, and morphological properties using a diverse set of techniques including nuclear magnetic resonance (NMR), Fourier transform infrared spectroscopy (FTIR), thermal gravimetric analysis (TGA), differential scanning calorimetry (DSC), X-ray scattering, and dielectric relaxation spectroscopy (DRS). Functionalization of native cellulose resulted in the

observation of a T_g, the values of which were inversely related to the size of the counteranion. Morphological analysis of the derivatives indicated that the materials were amorphous in nature, showing a clear nanophase separation dependent on the type of anion. By simply quaternizing the 1,2,3-triazole ring to produce the corresponding ionic moiety, the ionic conductivity of the material was increased by ~ 6-orders of magnitude at higher temperatures as compared to the native samples. Ionic conductivity was observed to have an Arrhenius (linear) behavior and was enhanced up to 4-orders of magnitude upon exposure to humidity. The results provided evidence to suggest that the thermal and ionic conductivity properties are dependent on anion basicity and hydration.

KEYWORDS: cellulose, poly(ionic liquid), ionic conductivity, morphology, X-ray scattering

INTRODUCTION

Naturally occurring and bio-inspired materials are of great interest for researchers working in a broad range of fields, from biochemistry and medicine to polymer and material science. As many of these materials derive themselves from relatively inexpensive and biorenewable sources of high abundance, having the ability to control the microstructure and/or composition could lead to novel bio-based materials. Furthermore, these materials could have broad applicability in a number of currently important areas of research, examples of which include biobatteries, tissue regeneration, and drug delivery vehicles.[1-3] Structural saccharide polymers, such as cellulose, interact through hydrophobic and electrostatic interactions, and the resulting matrices can exhibit useful and novel properties.[4-8] Cellulose is especially intriguing as it represents one of the most promising and readily available feedstocks for biobased monomers and functionalized

biomaterials.[9] Modifications of the cellulose backbone have led to a wider range of the thermal, mechanical, and morphological properties. For example, acylation of cellulose has led to improvements in organic solvent solubility and thermoplasticity, enabling its processing into a variety of end-use applications such as fabrics, films, and carbon dioxide separation membranes.[10-12]

One specific synthetic method that has been employed to modify cellulose and other polysaccharides is the 'click' 1,3-diploar cycloaddition between an alkyne and an azide.[13] The major advantage of using this type of a functionalization approach to make new polysaccharide-based biomaterials is the ease in which the cyclization can be done with little to no by-products.[14,15] Heinze and coworkers were one of the first groups to report the functionalization of cellulose using a copper-catalyzed cyclization strategy by reacting 6-deoxy-6-aminopropargylcellulose with a variety of azido-terminated reactants.[16] Evidence of successful cyclization was supported by FTIR and NMR spectroscopy. More recent applications of this chemistry toward the modification of cellulose and other polysaccharides have focused on the creation of new materials for biomedical applications. For example, Nada et al. crosslinked azido-functionalized ethyl cellulose electrospun fibers with propargyl-substituted cyclodextrin, generating materials that exhibited a high level of viability in human skin fibroblast cells.[17] Another recent report coupled azide-terminated cyclodextrin with alkyne-functionalized cellulose fibers.[18] The resulting materials showed promising antibacterial activity against *E. coli* and *S. aureu.*

Polymerized ionic liquids or poly(ionic liquid)s (PILs) are polymers synthesized with IL moieties covalently incorporated into the repeating unit.[19-23] As PILs retain some of the unique properties of ILs such as thermal and chemical stability, high ionic conductivity and tunable electrochemical properties while still possessing a polymeric solid state, they have been utilized

as ion conductive materials in electro-active devices and smart materials.[19,24,25] Ion transport in PILs has been related to a number of structural features, including the glass transition temperature (T_g), molecular weight, water content (humidity) and morphology of the polymer-counterion pair.[24-26] As the counterions (commonly anions) are the primary driving force for ionic conduction, species that are bulkier and non-coordinating tend to produce higher conduction by increasing free volume, reflected often in a lower T_g value, which facilitates ion hopping.[26] Additional enhancements in conductivity have been observed by increasing the concentration of ions in the polymer matrix.[27] Only a few reports have been published which demonstrate that ionic liquid groups can be covalently bound onto cellulose; however, none of these focused on ionic conductivity or the relationships that exist between polymer structure and morphology. In one example, Chen et al. prepared imidazolium-functionalized cellulose as catalysts for the cycloaddition of CO_2 with epoxides by reacting methyl imidazole with 6-chloro-6-deoxycellulose.[28] Imidazolium and ammonium-functionalized cellulosic materials have also been developed for carbon dioxide sorption.[29] Despite these reports of 1,2,3-triazole-functionalized cellulose, none of them went further to functionalize the *N*-3 position of the triazole ring. Tan et al. have demonstrated that 1,2,3-triazolium-functionalized starch materials can be prepared; however, these derivatives were synthesized to target potential antifungal properties rather than to investigate their ionic conductivity.[30,31]

PILs that contain a 1,2,3-triazolium unit in the repeating unit are often referred to as 1,2,3-triazolium poly(ionic liquid)s or TPILs. Drockenmuller and coworkers, pioneers in the area of TPILs, have recently reviewed their synthetic efforts, examples of which have included step-growth polyaddition of azides and alkynes and chain-growth polymerization of 1,2,3-triazolium-containing (meth)acrylic monomers.[32] Several covalently crosslinked networks have also been

reported, including TPIL epoxy−amine networks prepared from epoxy-functionalized IL monomers and a poly(propylene glycol)-based diamine. Relatively high anhydrous ionic conductivities were reported for these networks (~10^{-7} S/cm at 30 °C).[33] Additionally, thermally reversible C−N bond transalkylation exchanges have been utilized to prepare vitrimeric TPIL networks capable of being reshaped and recycled.[34,35] We have also explored the thermal, mechanical and conductive properties of TPIL polyester networks prepared using a carbon-Michael addition polymerization strategy.[36,37] Promising ionic conductivities (10^{-6} and 10^{-8} S/cm, 25 °C, 30% relative humidity (RH)) were found for these systems using electrochemical impedance spectroscopy.

Here, we report our initial efforts on the synthesis, ionic conductivity, and morphology of 1,2,3-triazolium-substituted cellulosic materials. Using the aforementioned azide-alkyne 'click' cyclization strategy, 1,2,3-triazolium groups were covalently bound to the backbone of cellulose with a high degree of substitution (> 90% per glucose unit). The impact of counteranion ([Br], [OTf], [NTf_2]) on the thermal and conductive properties of the materials was investigated. X-ray scattering profiles (SAXS/WAXS) were obtained for all of the materials studied here and correlations between structural changes and morphology are discussed. Additionally, the effect of humidity on ionic conductivity was explored since water plays a complex role in ion-transport, especially for hydrophilic counterions. Water can also assist in the disruption of hydrogen bonding, leading to plasticization and the formation of channels, both of which can enhance ion transport. Such behavior has been previously observed for silk/cellulose composites and poly(ionic liquid)s bearing hydrophilic ions;[38-42] however, to the best of our knowledge, no reports of this behavior in IL-functionalized cellulosic materials has been discussed. Thus, these materials are unique in that

a renewable, sustainable biomacromolecule in cellulose has been used as the foundational platform for novel, IL-functionalized conductive materials.

EXPERIMENTAL SECTION

General. All chemicals were purchased from Sigma-Aldrich or Acros Organics and were used as received without further purification. An ELGA Purelab® Ultra filtration device produced ultrapure water having a resistivity of 18 MΩ-cm. ^{1}H and ^{13}C NMR spectra were obtained on a JEOL-ECS 400 MHz spectrometer and reported chemical shift values were referenced to residual solvent signals (DMSO-d_6: ^{1}H, 2.50 ppm; ^{13}C, 39.52 ppm). Relevant NMR spectra (taken on 30 mg of sample in 0.75 mL of DMSO-d_6 at 80 °C, ^{1}H: 1200 scans; ^{13}C: 48000 scans) are included in the Supporting Information (**Figures S1-S8**). A PerkinElmer Spectrum Two™ FT-IR in transmission mode was utilized to record infrared spectra. The PerkinElmer Spectrum 10™ software was used to follow the desired peaks at 1 cm^{-1} resolution using 64 scans. A Perkin-Elmer 2400 CHNS/O Series II Elemental Analyzer was used to determine elemental composition (CHNS). Residual bromide content was determined by ion chromatography (ICS-1100, Dionex) as follows: an eluent concentration of 4.5 mM CO_3^{2-}/1.4mM HCO_3^- with a flow rate of 1.2 mL/min and a suppressor current of 31 mA. Chromatographic calibration was accomplished via the preparation and analysis of aqueous standards prepared by serial dilution of a 1000 ppm [Br] stock solution (from sodium bromide, Aldrich, > 99.9%). Each material (10 mg) was dissolved in 1 mL of acetonitrile:water (50:50 *v*:*v*) and injected. The amount of residual bromide in each anion exchanged sample was less than 0.8 % *w/w*.

Synthesis of azido-functionalized cellulose (CELL-N_3). Tosylate-functionalized cellulose was prepared according to a published procedure and the degree of substitution (DS) was found to be

0.95 based upon ^{1}H NMR spectroscopic analysis.[43] To a 500-mL round-bottomed flask was dissolved tosylate-functionalized cellulose (8.00 g, 0.0253 mol) in DMF (160 mL). Sodium azide (8.24 g, 0.127 mol) was added and the resulting solution was stirred at 100 °C for 24 hours. The reaction was then cooled to room temperature and slowly poured onto DI water (1 L). The precipitate was isolated and washed with DI water (2 x 300 mL), then crushed into a powder with a mortar and pestle, followed by additional washings with ethanol (3 x 300 mL). The wet solid was finally dried in a vacuum oven (< 0.1 mm Hg, 60 °C) overnight, producing a light brown powder (4.40 g, 93 %). ^{1}H and ^{13}C NMR spectra matched those which have been previously published.[16] The degree of substitution (DS) was determined to be 0.94 by elemental analysis (calculated from nitrogen-content). Anal. Calcd. for $C_6H_9N_3O_4$: C 38.51, H 4.85, N 22.45. Found: C 37.54, H 4.99, N 21.11.

Synthesis of 1,2,3-triazole-functionalized cellulose (CELL-triazole). To a 1-liter round-bottomed flask under argon was dissolved **CELL-N$_3$** (4.40 g, 0.0235 mol) in DMSO (500 mL). Solutions of copper sulfate (0.19 g in 35 mL DI water) and sodium ascorbate (0.47 g in 35 mL DI water) were added sequentially, followed by 1-heptyne (11.31 g, 0.118 mol). The resulting mixture was stirred at 50 °C for 72 hours, then cooled to room temperature and poured into DI water (1 L). The precipitate was isolated, washed with DI water (2 x 300 mL) and acetone (2 x 300 mL), then dried in a vacuum oven (< 0.1 mm Hg, 60 °C) overnight, yielding a light brown solid (6.10 g, 92 %). ^{1}H NMR (400 MHz, DMSO-d_6): δ 7.55-7.85 (1 H, triazole), 2.71-5.50 (AGU – anhydroglucose repeating unit), 2.55 (2 H, -*CH$_2$*-N), 1.50 (2 H, -*CH$_2$*-CH$_2$-N), 1.21 (4 H, -*CH$_2$*-*CH$_2$*-CH$_2$-CH$_2$-N), 0.48 (3 H, - *CH$_3$*). ^{13}C NMR (100 MHz, DMSO-d_6): δ 146.7, 122.5, 59.9-102.3 (C1-C5, AGU), 49.5 (C6, AGU), 30.4, 28.1, 24.7, 21.1, 13.3. The degree of substitution (DS) was

determined to be 0.93 by elemental analysis (calculated from nitrogen-content). Anal. Calcd. for $C_{13}H_{21}N_3O_4$: C 55.11, H 7.47, N 14.83. Found: C 54.11, H 8.01, N 13.85.

Synthesis of CELL-TRI-Br. CELL-triazole (5.40 g, 0.019 mol) was dissolved in DMF (120 mL) at 60 °C using a Teflon™ screw-capped pressure vessel (250 mL). Once dissolved, the solution was cooled to room temperature and ethyl bromide (20.7 g, 0.19 mol) was added and the resulting solution was warmed to 60 °C whereupon it was allowed to stir for 48 hours. The reaction was then cooled to room temperature and poured into acetone (400 mL). The precipitate was isolated, ground into a powder with a mortar and pestle, washed with additional acetone (3 x 250 mL) and dried overnight in a vacuum oven (< 0.1 mm Hg, 60 °C), resulting in a light brown powder (5.95 g, 80 %). ^{1}H NMR (400 MHz, DMSO-d_6): δ 8.79-9.21 (1 H, triazolium), 2.70-5.55 (AGU), 4.53 (2 H, -*CH*$_2$-N$^+$), 2.84 (2 H, -*CH*$_2$-N), 1.65 (2 H, -*CH*$_2$-CH$_2$-N), 1.49 (3 H, *CH*$_3$-CH$_2$-N$^+$), 1.38 (4 H, -*CH*$_2$-*CH*$_2$-CH$_2$-CH$_2$-N), 0.89 (3 H, *CH*$_3$-). ^{13}C NMR (100 MHz, DMSO-d_6): δ 143.4, 129.1, 53.4-102.3 (AGU), 46.1, 30.4, 27.1, 22.7, 21.1, 13.4. The degree of substitution (DS) was determined to be 0.92 by elemental analysis (calculated from nitrogen-content). Anal. Calcd. for $C_{15}H_{26}BrN_3O_4$: C 45.93, H 6.68, N 10.71. Found: C 41.75, H 6.86, N 9.85.

Synthesis of CELL-TRI-OTf. In a 50-mL round-bottomed flask was dissolved **CELL-TRI-Br** (1.00 g, 25.4 mmol) in DI water (10 mL). To this stirred solution was added a solution of lithium triflate (0.44 g, 28.0 mmol) in DI water (5 mL). The resulting solution was stirred at room temperature overnight. During this time a precipitate was observed to form. The precipitate was filtered, washed with DI water (3 x 25 mL), then dried in the vacuum oven (< 0.1 mm Hg, 60 °C) for 24 hours, resulting in 1.13 g of an off-white powder (96 %). ^{1}H NMR (400 MHz, DMSO-d_6): δ 8.70-8.91 (1 H, triazolium), 2.55-5.65 (AGU), 4.56 (2 H, -*CH*$_2$-N$^+$), 2.87 (2 H, -*CH*$_2$-N), 1.71 (2

H, -*CH*$_2$-CH$_2$-N), 1.54 (3 H, *CH*$_3$-CH$_2$-N$^+$), 1.38 (4 H, -*CH*$_2$-*CH*$_2$-CH$_2$-CH$_2$-N), 0.90 (3 H, *CH*$_3$-). ^{13}C NMR (100 MHz, DMSO-d_6): δ 143.6, 128.9, 120.5 (q, J = 325 Hz, -CF$_3$), 53.1-102.7 (AGU), 45.7, 30.1, 25.9, 22.0, 21.1, 13.0. The degree of substitution (DS) was determined to be 0.93 by elemental analysis (average DS calculated from nitrogen- and sulfur-content). Anal. Calcd. for $C_{16}H_{26}F_3N_3O_4S$: C 41.64, H 5.68, N 9.11, S 6.95. Found: C 40.20, H 7.85, N 8.97, S 6.21.

Synthesis of CELL-TRI-NTf$_2$. In a 50-mL round-bottomed flask was dissolved **CELL-TRI-Br** (1.00 g, 25.4 mmol) in DI water (10 mL). To this stirred solution was added a solution of lithium triflate (0.80 g, 28.0 mmol) in DI water (5 mL). The resulting solution was stirred at room temperature overnight. During this time a precipitate was observed to form. The precipitate was filtered, washed with DI water (3 x 25 mL), then dried in the vacuum oven (< 0.1 mm Hg, 60 °C) for 24 hours, resulting in 1.38 g of an off-white powder (91 %). ^{1}H NMR (400 MHz, DMSO-d_6): δ 8.59-9.00 (1 H, triazolium), 2.70-5.55 (AGU), 4.57 (2 H, -*CH*$_2$-N$^+$), 2.87 (2 H, -*CH*$_2$-N), 1.70 (2 H, -*CH*$_2$-CH$_2$-N), 1.54 (3 H, *CH*$_3$-CH$_2$-N$^+$), 1.39 (4 H, -*CH*$_2$-*CH*$_2$-CH$_2$-CH$_2$-N), 0.91 (3 H, *CH*$_3$-). ^{13}C NMR (100 MHz, DMSO-d_6): δ 143.6, 128.8, 119.2 (q, J = 322 Hz, -CF$_3$), 53.2-103.1 (AGU), 45.8, 30.1, 26.0, 22.0, 21.1, 13.1, 12.9. The degree of substitution (DS) was determined to be 0.97 by elemental analysis (average DS calculated from nitrogen- and sulfur-content). Anal. Calcd. for $C_{17}H_{26}F_6N_4O_8S_2$: C 34.46, H 4.42, N 9.46, S 10.82. Found: C 34.29, H 4.57, N 9.40, S 10.42.

Thermal Analysis. A TA Instruments Q200 Differential Scanning Calorimeter, equipped with an RSC90 cooling unit under a dry nitrogen gas flow of 50 mL/min was used to determine thermal transitions of cellulose and the 1,2,3-trizolium-substituted cellulosic materials. For standard DSC runs, a heating rate of 3 °C/min was conducted on 8-10 mg of sample using hermetically sealed aluminum pans. T_c values were determined at the maximum of the observed exothermic peak of the second heating event. Glass transition temperature (T_g) values were determined from the

inflection point of the reversible heat flow thermogram, produced from modulated DSC experiments (conditions: modulate ±1 °C for 60 s, ramp rate 3 °C/min from 0 to 250 °C).[44] A total of three replicate experiments were conducted for each material resulting in an average error of ± 2 °C in each T_g and T_c value. Thermal stability is defined by $T_{d5\%}$, the temperature at which 5% mass loss was observed, and was determined using a TA Instruments Q500. Samples (8-10 mg) were heated under dry nitrogen (30 mL/min) at a ramp rate of 10 °C/min from 30-800 °C. Duplicate experiments were completed on each sample, resulting in an error of ± 2 °C.

Anhydrous conductivity measurements. A TA Instruments DHR-2 Discovery Hybrid Rheometer with dielectric accessory and Keysight Technologies E4980AL/120 LCR meter was utilized. Samples (thickness of ~500 μm) were prepared by slow evaporation of a DMF solution of polymer (10-15 wt%) in a 12-mm diameter Teflon™ mold, clamped to a glass bottom treated with Rain-X®. The resulting film was placed in a vacuum oven (< 0.1 mm Hg, 60 °C) for 48-hours prior to testing. Once dried, each sample was placed between two 25-mm stainless steel, parallel plate electrodes in the environmental chamber, under a dry nitrogen atmosphere. The temperature was controlled using liquid nitrogen. Dielectric permittivity and conductivity were measured isothermally in 10 °C steps over a frequency range of 20.0-10^6 Hz with an ac amplitude of ± 0.01 V. A constant axial force of 5.0 ± 0.2 N was kept throughout each experiment and the sample was allowed to soak for 45 minutes at each temperature prior to obtaining measurements. The experiments were conducted at the highest desired temperature to ensure the best contact between the electrodes and sample. The DC-conductivity (σ_{DC}) was determined from the plateau value observed in the spectral dependence of the conductivity function ($\sigma' = \omega\varepsilon''\varepsilon_o$ where ω is the frequency, ε'' is the dielectric loss and ε_o is the vacuum permittivity). Duplicate polymers were

tested for each PIL ([Br], [OTf], [NTf_2]) and conductivity values were found to be reproducible within ± 1% uncertainty.

Conductivity measurements with humidity control. For experiments completed under a controlled humidity environment, DRS measurements were performed using an in-house, custom-built, two-electrode cell coupled to a Metrohm Autolab 302N potentiostat and FRA32M frequency response analyzer.[36] From each film (~500 μm thickness, prepared as described above) were cut circular disks (12 mm diameter). The sample was placed between the two stainless steel electrodes of the cell and the entire apparatus was then placed inside a controlled-temperature/humidity chamber (Espec BTU-433), set to the desired relative humidity (30, 50, or 70%). Dielectric permittivity and conductivity were measured isothermally over a frequency range of 0.1-10^7 Hz with an ac amplitude of ± 0.01 V in 10 °C steps. Samples were soaked at each individual temperature for 45-50 minutes in order to achieve a constant conductivity. As previously described, the DC-conductivity (σ_{DC}) was determined from the plateau value observed in the spectral dependence of the conductivity function ($\sigma' = \omega\varepsilon''\varepsilon_o$ where ω is the frequency, ε'' is the dielectric loss and ε_o is the vacuum permittivity).

Water uptake studies. Duplicate samples (thickness of ~500 μm) of each PIL were prepared by slow evaporation of a DMF solution of polymer (10-15 wt%) in a 12-mm diameter Teflon™ mold, clamped to a glass bottom treated with Rain-X®. Each sample (in triplicate, a total or six measurements for each PIL) was placed in the vacuum oven (< 0.1 mm Hg, 60 C) for 48-hours to ensure removal of all volatiles. Once dried, each sample was measured (w_{dry}), then placed in the controlled-temperature/humidity chamber (Espec BTU-433), set at 30 °C and to the desired relative humidity (30, 50 or 70%). The sample was allowed to equilibrate in the chamber until a constant mass was achieved (4-6 hours). This was defined as w_{wet}. Water uptake is defined as

(w_{wet}/w_{dry})*100. Standard deviation was determined across each set of three readings for each sample at each relative humidity.

X-ray scattering studies. The morphological studies were conducted using a dual environmental X-ray scattering system (DEXS) at the University of Pennsylvania. The Xeuss 2.0 by XENOCS has a Cu X-ray source, computer controlled focusing and transmission incident sample geometries, a 1M pixel Pilatus detector (2D), and a smaller detector for simultaneous small-angle scattering (SAXS) and wide-angle scattering (WAXS). A full flux collimation was used with a slit of 1.2 mm × 1.2 mm. Sample beam time was 300 seconds per run. The intensity reported is not absolute intensity and, thus, is reported in arbitrary units (a.u.). All samples were taped to a sample-holder and placed under vacuum during X-ray scattering characterization. The X-ray scattering profiles were evaluated using Foxtrot 3.4 and the isotropic 2-D scattering patterns were azimuthally integrated to yield intensity versus scattering vector.

RESULTS AND DISCUSSION

Avicel® PH-101 microcrystalline cellulose was first tosylated according to a previously published method (**Scheme 1**), resulting in a cellulosic material with degree of substitution (DS) of 0.95 (per AGU) as determined by ^{1}H NMR spectroscopy.[43] Further reaction with sodium azide led to 6-azidomethylcellulose (**CELL-N$_3$**). Copper-catalyzed azide-alkyne cyclization was then accomplished using 1-heptyne as the alkyne, leading to triazole-functionalized cellulose (**CELL-Tri**). Quaternization at the *N*-3 position was accomplished using an excess of ethyl bromide in DMF, resulting in the 1,2,3-triazolium bromide salt **CELL-TRI-Br** after isolation. Anion metathesis reactions were accomplished using the appropriate lithium salt (LiOTf or $LiNTf_2$) in high-purity DI water. In both cases, **CELL-TRI-OTf** and **CELL-TRI-NTf$_2$** were isolated as off-white salts with good yields (> 95 %). Analysis of the anion exchanged salts by ion

chromatography indicated that < 0.8 % (*w*/*w*) of bromide was present in each of the final materials. All of the 1,2,3-triazolium-functionalized cellulosic materials were found to exhibit a high degree of substitution (> 0.90 per AGU) as determined from elemental analysis data.

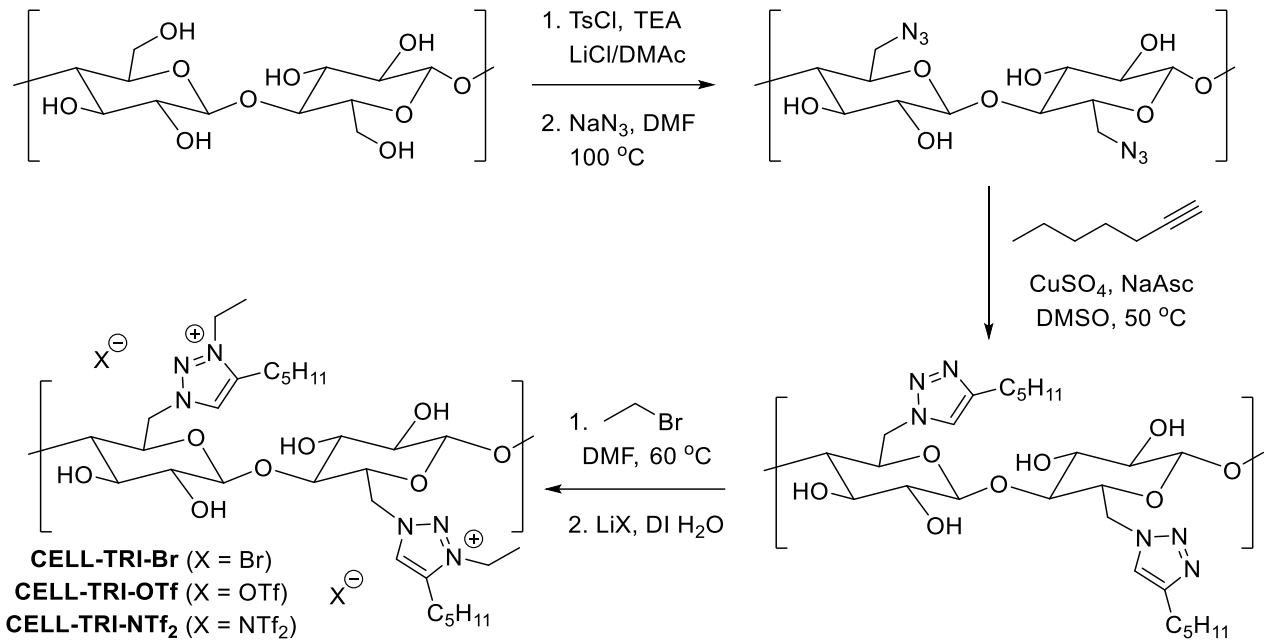

Scheme 1. Synthesis of 1,2,3-triazolium-functionalized cellulosic materials.

1,2,3-Triazolium-functionalized cellulosic materials were characterized by ^{1}H and ^{13}C NMR (**Figures S1-S8**) and FTIR spectroscopy. ^{1}H NMR analysis clearly showed the appearance of the proton of the triazole ring at ~7.7 ppm with the signal shifted downfield to ~8.7 ppm as a result of quaternization to 1,2,3-triazolium. Anion exchange reactions leading to the conversion of bromide to either [OTf] or [NTf_2] resulted in the appearance of a quartet at approximately 120 ppm in the ^{13}C NMR spectra, corresponding to the -CF_3 group (J ~ 325 Hz). Analysis of the FTIR data led to the following observations. Conversion of the azide to the 1,2,3-triazole ring was confirmed by the disappearance of the azide stretching vibration at 2110 cm^{-1} and the appearance of a new C=C stretching band at 1550 cm^{-1} (**Figure S9**). Quaternization of to the 1,2,3-triazolium

ring led to a slight shift in the C=C band to 1580 cm^{-1} (**Figure 1**).[45] Anion exchange of CELL-TRI-Br to the triflate analog led to new observed stretching bands at 1250 and 635 cm^{-1} (SO_3), as well as at 1150 cm^{-1} (CF_3).[45] Conversion to **CELL-TRI-NTf$_2$** led to the appearance of several new bands, including 1344, 1130, and 602 cm^{-1} (SO_2), 790 cm^{-1} (C-S) and 738 and 650 cm^{-1} (S-N-S).[45]

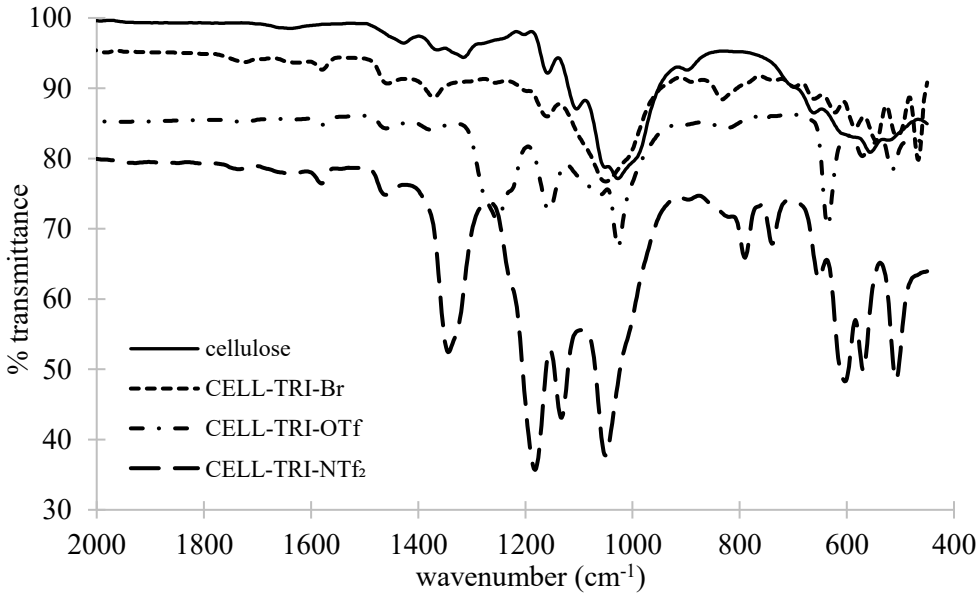

Figure 1. Overlay of FTIR spectra for cellulose and 1,2,3-triazolium-functionalized cellulosic derivatives.

Figure 2 shows DSC thermograms (second heating) for the three 1,2,3-triazolium-substituted cellulosic materials, as well as microcrystalline cellulose. Microcrystalline cellulose was observed to have a decomposition when heated above its melting point at 307 °C while the three 1,2,3-triazolium-containing materials exhibited both weak endothermic T_g and strong exothermic T_c crystallization (amorphous solid to crystalline solid) events (**Table 1**). Modulated DSC was utilized to confirm the existence of T_g values for the three IL-functionalized materials (as well as **CELL-triazole**, see **Figure S11**) by evaluating the reversible heat flow curves. The T_g and T_c transitions of the IL-functionalized cellulosic materials correlate inversely with

counteranion size on the order of [NTf_2] < [OTf] < [Br]. In addition to this relationship, the crystallization peak appears to broaden as the counteranion becomes larger. Large, non-coordinating counteranions such as [OTf] and [NTf_2] are hypothesized to partially plasticize the material by disrupting hydrogen bonding interactions and increasing segmental motion.

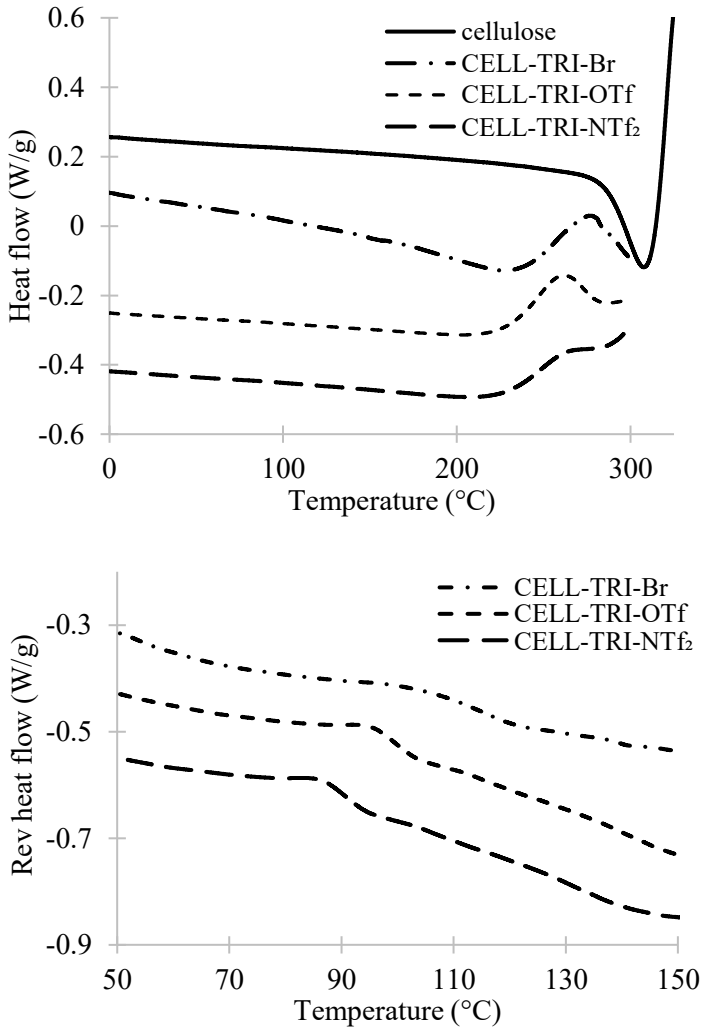

Figure 2. (top) Overlay of thermograms for cellulose and cellulose derivatives from standard DSC experimentation. (bottom) Overlay of reversing heat flow thermograms from modulated DSC experiments. All DSC experiments were done under anhydrous conditions using hermetically sealed pans.

Table 1. Thermal Properties of 1,2,3-Triazolium-substituted Cellulosic Materials.

material	DSC T_g (°C)	DSC T_c (°C)	TGA $T_{d5\%}$ (°C)
Cellulose	N/A	N/A	301
CELL-triazole	200	265	255
CELL-TRI-Br	113	276	187
CELL-TRI-OTf	101	265	219
CELL-TRI-NTf_2	90	264	240

Analysis of the 1,2,3-triazolium-substituted cellulosic materials by thermogravimetric analysis (TGA) revealed that all three salts were less thermally stable than microcrystalline cellulose (**Figure 3**). Addition of the triazole substituent to cellulose resulted in a lowering of the $T_{d5\%}$ value by almost 50 °C. Further quaternization of the triazolium ring led to an additional reduction in $T_{d5\%}$ value. This is presumably due to the introduction of a known decomposition pathway, the reverse S_N2 (Menshutkin) reaction via the side chain 1,2,3-triazolium ring. Such a decomposition event has been observed for a variety of ammonium, imidazolium and phosphonium ionic liquids and poly(ionic liquid)s.[46] As further supported in the derivative weight loss plots (**Figure S10**), the initial mass loss for all three cellulose PILs is large enough (35-45% mass loss) to account for the loss of the substituted 1,2,3-triazole ring via the reverse Menshutkin reaction as the main decomposition; however, it is worth noting that the derivative plots show other decomposition events occurring as temperature increases. Within the three-salt series, thermal stability was observed to increase with decreasing Lewis basicity of the anion on the order of [Br] < [OTf] < [NTf_2]. This relationship is analogous to what has been previously observed with other 1,2,3-triazolium-containing PILs.[32,36,37]

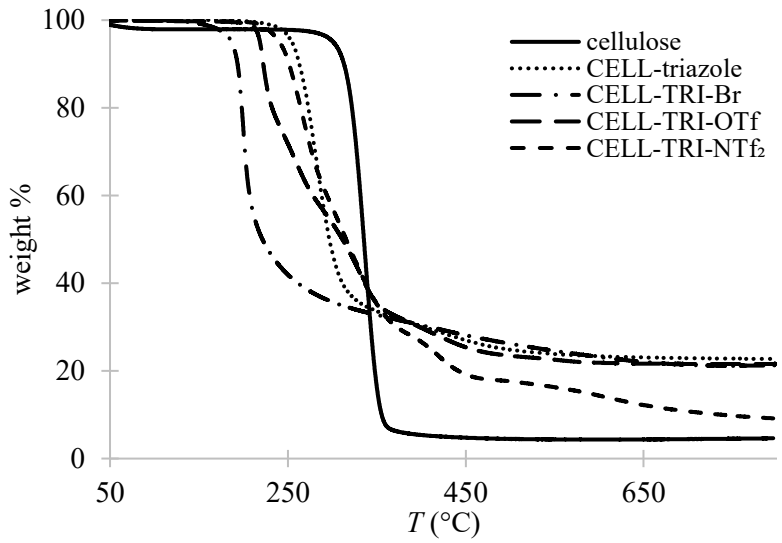

Figure 3. Overlay of TGA thermograms for cellulose and the 1,2,3-triazolium-substituted cellulosic derivatives.

Anhydrous, isothermal conductivity measurements were completed in 10 °C steps (150 to 30 °C) on PIL films which were ~ 300 μm in thickness. The sample was allowed to equilibrate for 45 minutes at each of the desired temperatures prior to obtaining data. As **CELL-TRI-Br** exhibited a relatively low thermal stability (TGA T_{onset} = 152 °C), the upper temperature of the experiment was started at 130 °C to avoid complications arising from possible decomposition. As shown in **Figure 4**, ionic conductivity was found to be on the order of 10^{-8} to 10^{-10} S/cm at 30 °C. In comparing the three 1,2,3-triazolium-substituted materials, an inverse relationship between ionic conductivity and T_g was observed. Larger, hydrophobic anions such as [OTf] and [NTf_2] are involved in weaker ionic interactions and thus allow for an increase in free volume and segmental motion. As a control, the same experiment was conducted on samples of Fisherbrand® filter paper (cellulose) and **CELL-Tri**. Neither sample was observed to have appreciable conductivity (< 10^{-10} S/cm) *at 150 °C* and conductivity was generally undetectable below 120 °C (**Figures S14,S15**). Thus, by simply quaternizing the 1,2,3-triazole ring to produce the corresponding ionic moiety,

the ionic conductivity of the material was increased by ~ 6-orders of magnitude at higher temperatures.

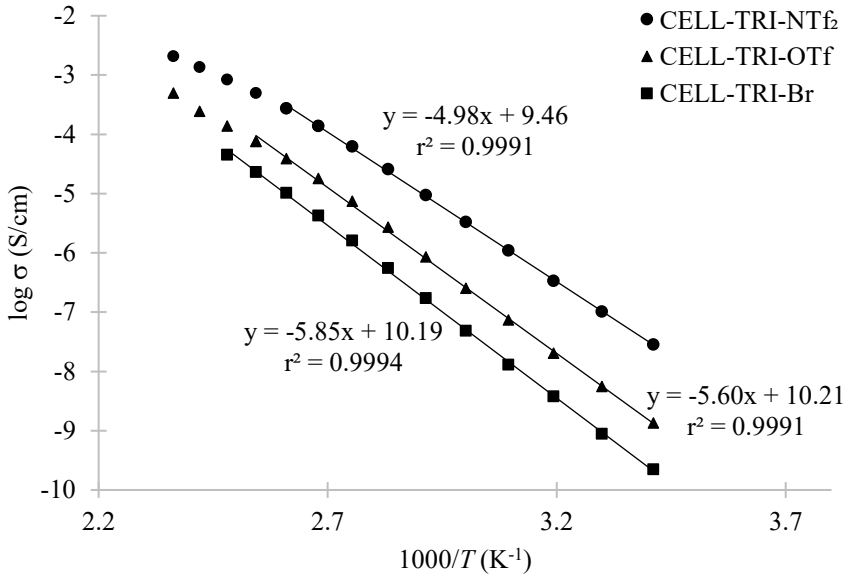

Figure 4. Overlay of ionic conductivities of 1,2,3-triazolium-substituted cellulosic materials as a function of temperature.

In general, PILs rely on the "hopping" of free ions along the backbone of the polymer and can exhibit linear (Arrhenius) and/or non-linear (Vogel-Fulcher-Tamman) responses to temperature.[47-50] All three of the 1,2,3-triazolium-substituted materials tested in this study exhibited primarily Arrhenius-like behavior, which is commonly observed when the ionic conductivity is measured near to or below the T_g. This linear response accounts for the thermal "hopping" frequency of ions as compared to the contributions of other aspects of the polymer such as segmental motion and relaxation events, both of which lead to a more non-linear (VFT) response.[48-50] **CELL-TRI-Br** exhibited excellent Arrhenius behavior (r^2 > 0.9996) with an activation energy of 112 kJ/mol while **CELL-TRI-OTf** and **CELL-TRI-NTf$_2$** exhibited near-linear behavior at or below the T_g (< 110 °C). Above this temperature, some curvature (VFT

behavior) in the data can be observed. Arrhenius fits to the linear portions of the [OTf] and [NTf_2] polymers ($r^2 > 0.9990$) led to activation energies of 107 kJ/mol and 95 kJ/mol, respectively. These values correlate with the ion association capability of the counterion. In other words, the thermal barrier to ion hopping for bromide is the highest because it is the most Lewis basic, thus forming relatively strong associations with the corresponding 1,2,3-triazolium cation.

To probe the effect of ionic liquid-functionalization and counteranion choice on the morphology of the resulting films, X-ray scattering data was acquired. **Figure 5** shows the X-ray scattering profile for the WAXS and SAXS regions as a function of scattering vector (q) for all of the 1,2,3-triazolium-functionalized cellulosic derivatives plus the neutral **CELL-triazole** polymer and Avicel® microcrystalline cellulose. Qualitatively, the results show a change in morphology after functionalization and quaternization. The typical sharp crystallite reflections, which are characteristics of native microcrystalline cellulose Iβ, are not observed in the neutral polymer **CELL-triazole** nor in the IL-functionalized materials, regardless of anion type.[51,52] Instead, these polymers show a broad scattering peak at high q values which is indicative of an amorphous structure.[53] The X-ray scattering profile for all of the 1,2,3-triazolium-functionalized cellulosic derivatives, including the neutral polymer, show two distinct scattering peaks. **CELL-TRI-NTf_2** exhibits a third scattering peak. The scattering vector positions and correlation lengths (d_x), calculated using the equation $d_x = 2\pi/q_x$ where x is b, pil or s, associated with each peak are shown in **Table 2**.

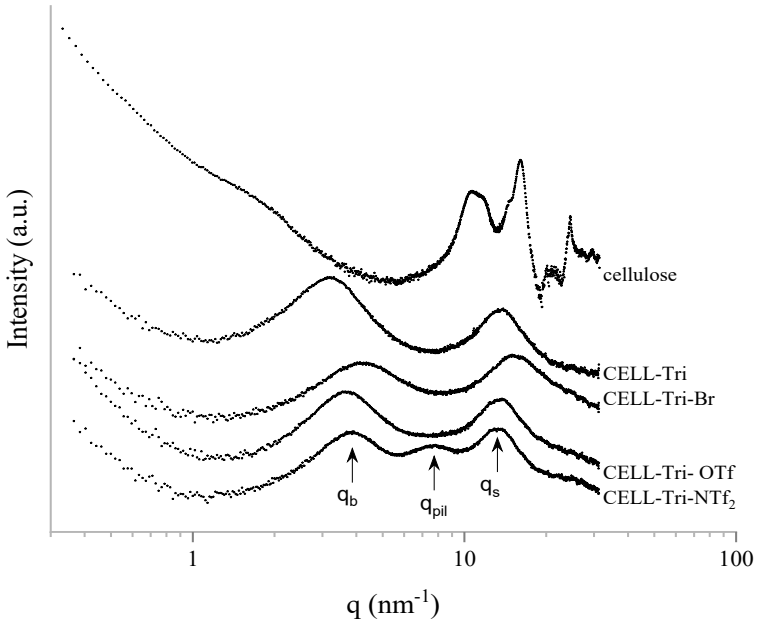

Figure 5. WAXS/SAXS combined X-ray scattering as a function of scattering vector for the 1,2,3-triazolium-functionalized cellulosic materials and microcrystalline cellulose.

Table 2. Scattering vectors (q_x) and calculated correlation lengths (d_x) for each observable peak, obtained from WAXS/SAXS combined x-ray scattering profiles.

material	q_s (nm^{-1}) d_s (nm)	q_{pil} (nm^{-1}) d_{pil} (nm)	q_b (nm^{-1}) d_b (nm)
CELL-triazole	13.80 0.45	--	3.25 1.93
CELL-TRI-Br	15.40 0.41	--	4.30 1.46
CELL-TRI-OTf	13.50 0.46	--	3.70 1.70
CELL-TRI-NTf_2	13.32 0.47	7.72 0.81	3.90 1.61

The high scattering vector q_s is the amorphous halo and is generally attributed to the interaction between side chains or pendant group in the polymers.[53] This correlation length is also attributed to interactions between the backbone and cation/anion pairs apart from the neutral polymer because it does not have any ions. Its correlation distances range from 0.41 to 0.47 nm and it is dependent on the type of anion. As the anion complexity, size and number of interaction points increases, this distance increases as well. The low q, q_b, for all of the polymers, including the neutral polymer, is related to the correlation distance between backbone-to-backbone in the polymer melt. The low q, q_b, for all of the PILs, as well as for the neutral polymer, is related to the correlation distance between backbone-to-backbone spacing in the polymer. This finding is similar to what was observed for a vinyl imidazolium-based PIL bearing a short (ethyl) alkyl chain length. This polymer, studied by Colby and others, has been analyzed morphologically and atomistically, the results of which assigned this low q value to the backbone-to-backbone distance.[53-57] The length scale (1.61 to 1.93 nm) was also found to be very similar to other PIL systems with cyclic pendant groups,[54-56] As with these other PILs, the intensity and broadness of the peaks are associated with a degree of nanophase separation that depends on the type of anion and the degree of side chain interdigitation (related to polarity).

The mid scattering vector q_{pil}, is associated with the distance between neighboring ionic groups (anion-anion and cation-cation). In comparing the neutral polymer with the other PILs one can notice frequency changes (noise) in this region as a function of anion type. This means that as the electron density difference between ions increases, this correlation length becomes more apparent as was observed for **CELL-TRI-NTf$_2$**. The correlation distance, d_{pil}, for **CELL-TRI-NTf$_2$** is 0.81 nm, the length scale of which is typical as to other PIL systems with different sidechains and anions.[53,54,56,57] **Figure 6** shows a representation of the backbone-to-backbone and

polymerized ionic species correlation length as depicted from the cellulose dimers and their interactions.

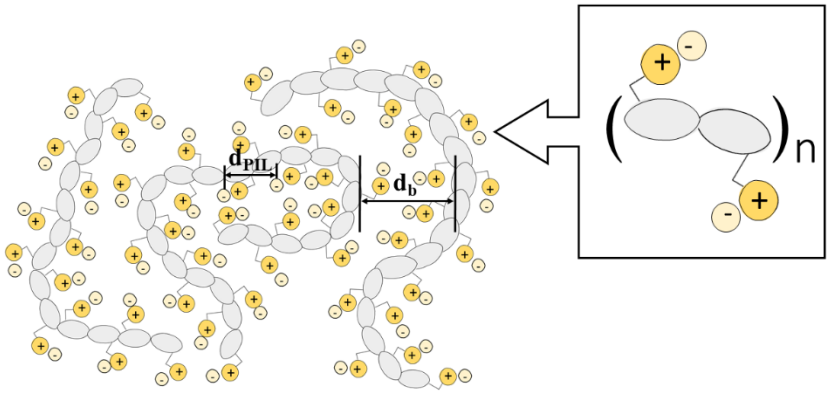

Figure 6. Representation of the 1,2,3-triazolium-functionalized cellulosic materials, including a schematic depiction for d_b and d_{pil}.

The effect of humidity on the ionic conductivity of the IL-functionalized cellulosic materials was analyzed by taking a circular disk (12 mm diameter, 300 μm thickness) of each film and measuring the dielectric permittivity and conductivity isothermally in 10 °C steps from 30-90 °C at the appropriate relative humidity (30, 50 or 70%). All three of the IL-functionalized cellulosic materials experienced an enhancement in ionic conductivity as a function of increasing humidity (**Figure 7**). At 70% RH, CELL-Br exhibited the largest increase in ionic conductivity of approximately four orders of magnitude, while CELL-OTf and CELL-NTf_2 each experienced a slightly lower enhancement of 2-3 orders of magnitude.

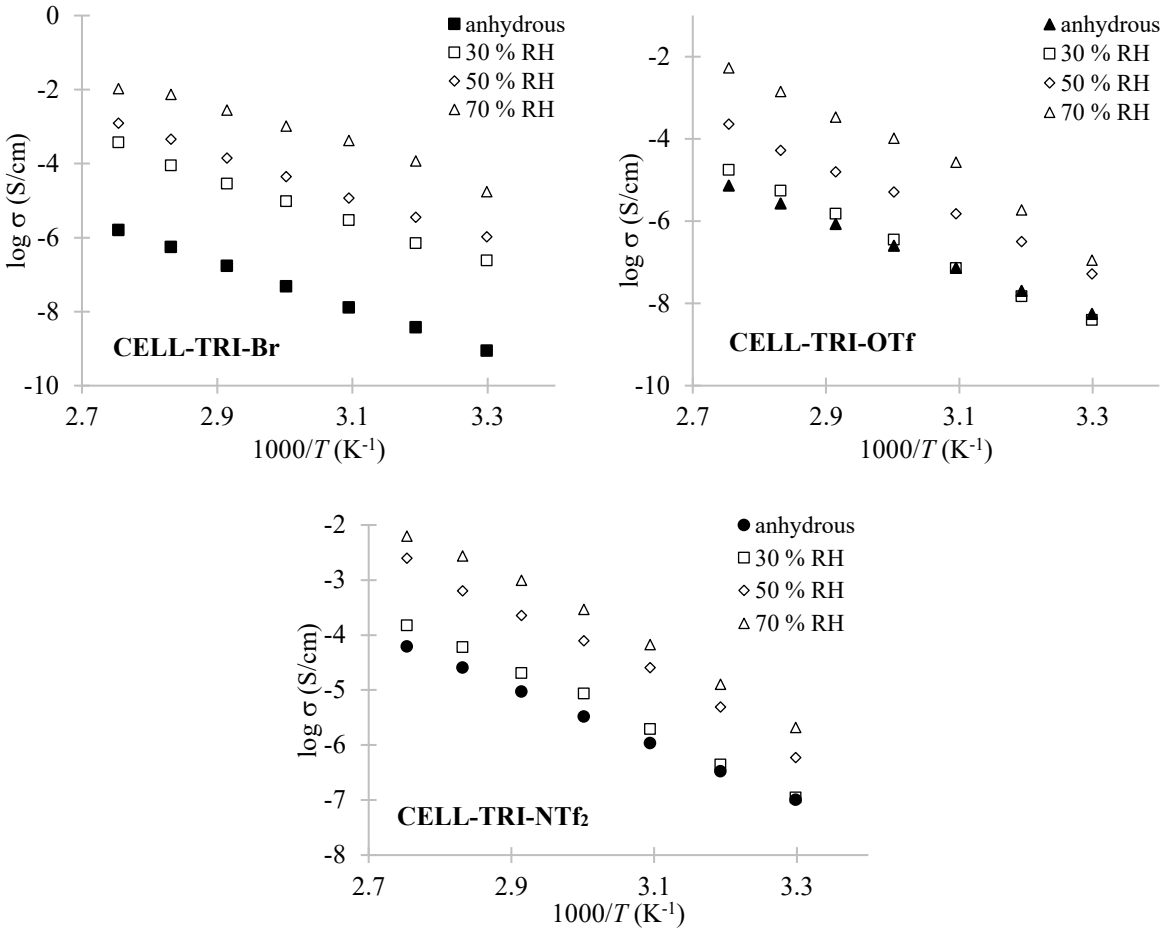

Figure 7. Influence of relative humidity on the ionic conductivity of 1,2,3-triazolium-functionalized cellulosic materials as a function of temperature. Filled shapes represent the original, anhydrous conductivity data, acquired using the rheometer (refer to **Figure 4**). The empty shapes represent conductivity values taken at various relative humidity conditions: 30 % (□), 50 % (◊) and 70 % (Δ).

To complement this study, water uptake was determined for each material at 30 °C as a function of RH (**Table 3**). Samples were placed in a humidity-controlled oven and allowed to equilibrate for 6 hours (further equilibration time did not result in any additional water absorption). As **CELL-TRI-Br** employs the most hydrophilic counteranion, in combination with the hydrophilic cellulosic backbone, it was not surprising that this material was found to exhibit the

highest water uptake (> 80% water uptake at 70% RH). However, even the materials bearing the more hydrophobic anions ([OTf] and [NTf_2]) were found to absorb a small amount of water (3-7 %) across all humidity conditions, presumably due to the natural affinity that cellulose has for water.[38] When present, regardless of counteranion, water acts as a plasticizer in these systems, disrupting hydrogen bonding and creating channels that could enhance ion transport. **Figure 6** shows the possible ion channels separated by the cellulose backbones. To rule out these enhancements being due to simple T_g-shifts, T_g-normalized plots were assembled and very little coalescence of the curves was observed (**Figure S17**). Thus, it is hypothesized that, at a critical water concentration, these spacings increase and water-assisted ion-transport may be possible.

Although the data presented here does not directly support water-assisted ion transport and additional experiments are necessary, it is worth noting that enhanced ion transport in silk and silk/cellulose composites has been previously observed when exposed to water, resulting in increases in ionic conductivity.[39,40,58] PILs have also shown enhancements in ionic conductivity in the presence of water, especially when the counteranion is hydrophilic (halides, hydroxide, alkoxides, or other smaller inorganic anions). For example, Elabd and coworkers observed a 3- to 4-fold enhancement in bromide conductivity for a series of imidazolium-containing block copolymers.[41,42] It was hypothesized that, as humidity increased, the water absorbed by the polymer created microchannels, an observation supported by X-ray scattering data. The lack of coalescence in the T_g-normalized ionic conductivity curves for the cellulosic PILs reported here may be indicative of a similar water-assisted process.

Table 3. Water uptake data for each 1,2,3-triazolium-functionalized cellulosic material as a functional of relative humidity at 30 °C after 6 hours.

material	30 % RH	50 % RH	70 % RH
CELL-TRI-Br	60.9 ± 1.2 %	79.5 ± 7.6 %	83.4 ± 9.0 %
CELL-TRI-OTf	4.3 ± 1.5 %	7.1 ± 0.8 %	8.2 ± 1.1 %
CELL-TRI-NTf_2	2.7 ± 1.0 %	5.7 ± 1.0 %	7.3 ± 1.1 %

CONCLUSIONS

Cellulose is an inexpensive and sustainable raw material which, when functionalized with an ionic liquid unit, could serve as an important foundational polymer for new PILs. Several 1,2,3-triazolium-functionalized cellulosic materials were prepared using azide-alkyne 'click' cyclization, followed by quaternization. Three counteranions ([Br], [OTf] and [NTf_2]) were chosen to determine the range of properties available through this simple substitution strategy. Substitution of the 1,2,3-triazolium ring onto the cellulose backbone led to a disruption of hydrogen bonding and an increase in free volume and segmental motion, leading to the observance of a T_g (inversely dependent on ion size). Functionalization of the cellulose, however, led to a decrease in thermal stability, as observed using TGA.

Simple inclusion of a 1,2,3-triazolium group onto each AGU (> 0.9 DS) led to a 6- to 8-orders of magnitude increase in anhydrous ionic conductivity when compared to native cellulose or to the 1,2,3-triazole-substituted cellulose at 130 °C. Exposure of each of the PIL materials to a controlled humidity environment led to even further increases in ionic conductivity. X-ray scattering profiles indicated a loss of the distinct crystallization reflections of the native cellulose upon quaternization, indicating an amorphous structure. Two main scattering peaks, one

representing the amorphous halo and the other representing the backbone-to-backbone distance, were observed for each functionalized cellulosic materials. **CELL-TRI-NTf$_2$** exhibited a third scattering peak (q_{pil}) which was attributed to the distance between neighboring ionic groups. Although additional work needs to be completed to fully understand the complex relationships that exist between morphology, water uptake and ionic conductivity, this study demonstrates a new and exciting area of research for cellulose, one that is potentially sustainable while also being important to energy-related applications.

ASSOCIATED CONTENT

Supporting Information. Relevant ^{1}H and ^{13}C NMR spectra, as well as FTIR spectra for cellulose, azido-functionalized cellulose and 1,2,3-triazolium-functionalized cellulose, are included. Also provided are the DSC reverse heat flow thermogram for the 1,2,3-triazolium-substituted cellulose and examples of anhydrous ionic conductivity data (log σ′ vs. ω plots).

AUTHOR INFORMATION

Corresponding Author

Dr. Kevin M. Miller

1201 Jesse D. Jones Hall

Department of Chemistry

Murray State University

Murray, KY 42017

e-mail: kmiller38@murraystate.edu

Author Contributions

The manuscript was written through contributions of all authors. All authors have given approval to the final version of the manuscript.

ACKNOWLEDGEMENTS

R.M. and K.M.M. would like to acknowledge support for this project from the Murray State University McNair Scholars Program. Acknowledgement to the National Science Foundation (MRI award # DMR-18-28251) and to the Department of Chemistry at Murray State University for partial financial support is made by R.M., V.M.S., S.M.B. and K.M.M. S.A.L. and D.S.C. want to acknowledge the funding provided by the National Science Foundation Grant (DMR 1809354), and Rutgers University laboratory start-up funds. We would like to thank people working at the LRSM at the University of Pennsylvania, including Prof. Paul Heiney for the training and use of X-ray Scattering equipment (DEXS). The DEXS is funded by ARO DURIP (W911NF-17-1-02822), NSF-MRI (17-25969), NSF-MRSEC (17-20530), and University of Pennsylvania.

REFERENCES

1. Colo, F.; Bella, F.; Nair, J. R.; Destro, M.; Gerbaldi, C. Cellulose-Based Novel Hybrid Polymer Electrolytes for Green and Efficient Na-Ion Batteries. *Electrochim. Acta* **2015,** *185*, 185-190.

2. Barud, H. O.; Barud, H.; Cavicchioli, M.; de Amaral, T. S.; de Olivera Jr., O B.; Santos, D. M.; Peterson, A. L.; Celes, F.; Borges, V. M.; de Olivera, C. I.; de Olivera, P. F.; Furtaso, R. A.;

Tavares, D. C.; Bibeiro, S. J. L. Preparation and Characterization of a Bacterial Cellulose/Silk Fibroin Sponge Scaffold for Tissue Regeneration. *Carbohydr. Polym.* **2015,** *128*, 41-51.

3. Lamboni, L.; Gauthier, M.; Yang, G; Wang, Q. Silk Sericin: A Versatile Material for Tissue Engineering and Drug Delivery. *Biotech. Adv.* **2015,** *33*, 1855-1867.

4. Freddi, G.; Romano, M.; Massafra, M. R.; Tsukada, M. Silk Fibroin/Cellulose Blend Films: Preparation, Structure, and Physical Properties. *J. Appl. Polym. Sci.* **1995,** *56*, 1537-1545.

5. Zhou, L.; Wang, Q.; Wen, J.; Chen, X.; Shao, Z. Preparation and Characterization of Transparent Silk Fibroin/Cellulose Blend Films. *Polymer* **2013,** *54*, 5035-5042.

6. Wongpanit, P.; Sanchavanakit, N.; Pavasant, P.; Bunaprasert, T.; Tabata, Y.; Rujiravanit, R. Preparation and Characterization of Chitin Whisker-Reinforced Silk Fibroin Nanocomposite Sponges. *Eur. Polym. J.* **2007,** *43*, 4123-4135.

7. Tran, C. D.; Mututuvari, T.M. Cellulose, Chitosan and Keratin Composite Materials: Facile and Recyclable Synthesis, Conformation and Properties. *ACS Sustainable Chem. Eng.* **2016,** *4*, 1850-1861.

8. Boy, R.; Narayanan, G.; Chung, C. C.; Kotek, R. Novel Cellulose-Collagen Blend Biofibers Prepared from an Amine/Salt Solvent System. *Int. J. Biol. Macromol.* **2016,** *92*, 1197-1204.

9. O'Dea, R. M.; Willie, J. A.; Epps, III, T. H. 100th Anniversary of Macromolecular Science Viewpoint: Polymers from Lignocellulosic Biomass. Current Challenges and Future Opportunities. *ACS Macro Lett.* **2020,** *9*, 476-493.

10. Klemm, D.; Heublein, B.; Fink, H.-P.; Bohn, A. Cellulose: Fascinating Biopolymer and Sustainable Raw Material. *Angew. Chem. Int. Ed.* **2005,** *44*, 3358-3393.

11. Zheng, X. Y.; Gandour, R. D.; Edgar, K. J. TBAF-Catalyzed Deacylation of Cellulose Esters: Reaction Scope and Influence of Reaction Parameters. *Carbohydr. Polym.* **2013,** *98*, 692-698.

12. Mulder, M. *Basic Principles of Membrane Technology*, 2nd ed., Springer Netherlands, 1996.

13. Elchinger, P.-H.; Faugeras, P.-A.; Boëns, B.; Brouillette, F.; Montplaisir, D.; Zerrouki, R.; Lucas, R. Polysaccharides: The "Click" Chemistry Impact. *Polymers* **2011,** *3*, 1607-1651.

14. Kolb, H. C.; Finn, M. G.; Sharpless, K. B. Click Chemistry: Diverse Chemical Function from a Few Good Reactions. *Angew. Chem. Int. Ed.* **2001,** *40*, 2004-2021.

15. Meldal, M.; Tornøe, C. W. Cu-Catalyzed Azide-Alkyne Cycloaddition. *Chem. Rev.* **2008,** *108*, 2952-3015.

16. Leibert, T.; Hansch, C.; Heinze, T. Click Chemistry with Polysaccharides. *Macromol. Rapid Commun.* **2006,** *27*, 208-213.

17. Nada, A. A.; Abdellatif, F. H. H.; Ali, E. A.; Abdelazeem, R. A.; Soliman, A. A. S.; Abou-Zeid, N. Y. Cellulose-Based Click-Scaffolds: Synthesis, Characterization and Biofabrications. *Carbohydr. Polym.* **2018,** *199*, 610-618.

18. Sun, L.; Xiao, G.; Qian, X.; An, X. Alkyne Functionalized Cellulose Fibers: A Versatile "Clickable" Platform for Antibacterial Materials. *Carbohydr. Polym.* **2019,** *207*, 68-78.

19. Yuan, J.; Mecerreyes, D.; Antonetti, M. Poly(Ionic Liquid)s: An Update. *Prog. Polym. Sci.* **2013**, *38*, 1009-1036.

20. Yuan, J.; Antonietti, M. Poly(Ionic Liquid)s: Polymers Expanding Classical Property Profiles. *Polymer* **2014**, *52*, 1469-1482.

21. Shaplov, A. S.; Marcilla, R.; Mecerreyes, D. Recent Advances in Innovative Polymer Electrolytes based on Poly(Ionic Liquid)s. *Electrochim. Acta* **2015**, *175*, 18-34.

22. Qian, W.; Texter, J.; Yan, F. Frontiers in Poly(ionic liquid)s: Syntheses and Applications. *Chem. Soc. Rev.* **2017,** 46, 1124-1159

23. Bara, J. E.; O'Harra, K. E. Recent Advances in the Design of Ionenes: Toward Convergence with High-Performance Polymers. *Macromol. Chem. Phys.* **2019,** *220*, 1900078.

24. Matsumi, N.; Sugai, K.; Miyake, M.; Ohno, H. Polymerized Ionic liquids via Hydroboration Polymerization as Single Ion Conductive Polymer Electrolytes. *Macromolecules* **2006,** *39*, 6924-6927.

25. Jia, Z.; Lei, Q.; He, F.; Zheng, C.; Liu, Y.; Zhao, X.; Yin, J. Interfacial Polarization and Electroresponsive Effect of Anionic and Cationic Poly(ionic liquid)s. *ACS Appl. Polym. Mater.* **2019,** *1*, 2862-2874.

26. Takeoka, S.; Ohno, H.; Tsuchida, E. Recent Advancement of Ion-conductive Polymers. Recent Advancement of Ion-Conductive Polymers. *Polym. Adv. Tech.* **1993,** *4*, 53-73.

27. Klein, R.; Zhang, S.; Dou, S.; Jones, B. H.; Colby, R. H.; Runt, J. Modeling Electrode Polarization in Dielectric Spectroscopy: Ion Mobility and Mobile Ion Concentration of Single-Ion Polymer Electrolytes. *J. Chem. Phys.* **2006,** *124*, 144903.

28. Chen, Q.; Peng, C.; Xie, H.; Zhao, Z. K.; Bao, M. Cellulosic Poly(ionic liquid)s: Synthesis, Characterization and Application of CO_2 to Epoxides. *RSC Adv.* **2015,** *5*, 44598-44603.

29. Bernard, F. L.; Duczinski, R. B.; Rojas, M. F.; Fialho, M. C. C.; Carreno, L. A.; Chaban, V. V.; Vecchia, F. D.; Einloft, S. Cellulose Based Poly(ionic liquid)s: Tuning Cation-Anion Interaction to Improve Carbon Dioxide Sorption. *Fuel* **2018,** *211*, 76-86.

30. Tan, W.; Li, Q.; Gao, Z.; Qiu, S.; Dong, F.; Guo, Z. Design, Synthesis of Novel Starch Derivative Bearing 1,2,3-Triazolium and Pyridinium and Evaluation of its Antifungal Activity. *Carbohydrate Polym.* **2017,** *157*, 236-243.

31. Tan, W.; Li, Q.; Dong, F.; Qiu, S.; Zhang, J.; Guo, Z. Novel 1,2,3-Triazolium-Functionalized Starch Derivatives: Synthesis, Characterization, and Evaluation of Antifungal Property. *Carbohydrate Polym.* **2017,** *160*, 163-171.

32. Obadia, M. M.; Drockenmuller, E. Poly(1,2,3-triazolium)s: A New Class of Functional Polymer Electrolytes. *Chem. Commun.* **2016,** *52*, 2433−2450.

33. Nguyen, T. K. L.; Obadia, M. M.; Serghei, A.; Livi, S.; Duchet-Rumeau, J.; Drockenmuller, E. 1,2,3-Triazolium-Based Epoxy-Amine Networks: Ion-Conducting Polymer Electrolytes. *Macromol. Rapid Commun.* **2016,** *37*, 1168−1174.

34. Obadia, M. M.; Jourdain, A.; Cassagnau, P.; Montarnal, D.; Drockenmuller, E. Tuning the Viscosity Profile of Ionic Vitrimers Incorporating 1,2,3-Triazolium Cross-links. *Adv. Funct. Mater.* **2017,** *27*, 1703258.

35. Obadia, M. M.; Mudraboyina, B. P.; Serghei, A.; Montarnal, D.; Drockenmuller, E. Reprocessing and Recycling of Highly Cross-Linked Ion-Conducting Networks Through Transalkylation Exchanges of C−N Bonds. *J. Am. Chem. Soc.* **2015,** *137*, 6078−6083.

36. Nguyen, A.; Rhoades, T. C.; Johnson, R. D.; Miller, K. M. Influence of Anion and Crosslink Density on the Ionic Conductivity of 1,2,3-Triazolium-based Poly(ionic liquid) Polyester Networks. *Macromol. Chem. Phys.* **2017,** *218*, 1700337

37. Tracy, C. A.; Adler, A. M.; Nguyen, A.; Johnson, R. D.; Miller K. M. Covalently Crosslinked 1,2,3-Triazolium-Containing Polyester Networks: Thermal, Mechanical, and Conductive Properties. *ACS Omega*, **2018,** *3*, 13442-13453.

38. Lindman, B.; Karlstrom, G.; Stigsson, I. On the Mechanism of Dissolution of Cellulose. *J. Mol. Liq.* **2010,** *156*, 76-81.

39. Yazawa, K.; Ishida, K.; Masunaga, H.; Hikima, T.; Numata, K. Influence of Water Content on the β-Sheet Formation, Thermal Stability, Water Removal, and Mechanical Properties of Silk Materials. *Biomacromolecules* **2016,** *17*, 1057-1066.

40. Solin, K.; Borghei, M.; Sel, O.; Orelma, H.; Johansson, L.-S.; Perrot, H.; Rojas, O. J. Electrically Conductive Thin Films Based on Nanofibrillated Cellulose: Interactions with Water and Applications in Humidity Sensing. *ACS Appl. Mater. Interfaces* **2020,** *12*, 36437-36448.

41. Elabd, Y. A. Ion Transport in Hydroxide Conducting Block Copolymers. *Mol. Syst. Des. Eng.* **2019,** *4*, 519-530.

42. Meek. K. M.; Sharick, S.; Ye, Y.; Winey, K. I.; Elabd, Y. A. Bromide and Hydroxide Conductivity-Morphology Relationships in Polymerized Ionic Liquid Block Copolymers. *Macromolecules* **2015,** *48*, 4850-4862.

43. Rahn, K.; Diamantoglou, M.; Berghmans, H.; Heinze, T. Synthesis, Characterization and Properties of Methylaminecellulose. *Angew. Makromol. Chem.* **1996,** *238*, 143-163.

44. Picker, K. M.; Hoag, S. W. Characterization of the Thermal Properties of Microcrystalline Cellulose by Modulated Temperature Differential Scanning Calorimetry. *J. Pharm. Sci.* **2002,** *91*, 342-349.

45. Paschoal, V. H.; Faria, L. F. O.; Riberio, M. C. C. Vibrational Spectroscopy of Ionic Liquids. *Chem. Rev.* **2017,** *117*, 7053-7112.

46. Williams, S. R.; Long, T. E. Recent Advances in the Synthesis and Structure-Property Relationships of Ammonium Ionenes. *Prog. Polym. Sci.* **2009,** *34*, 762-782.

47. Keith, J. R.; Rebello, N. J.; Cowen, B. J.; Ganesan, V. Polymerized Ionic Liquids: Correlation of Ionic Conductivity with Nanoscale Morphology and Counterion Volume. *ACS Macro Lett.* **2019,** *8*, 387-392.

48. Chen, H.; Choi, J.; Salas-de la Cruz, D.; Winey, K. I.; Elabd, Y. A. Polymerized Ionic Liquids: The Effect of Random Copolymer Composition on Ion Conduction. *Macromolecules* **2009,** *42*, 4809-4816.

49. Fragiadakis, D.; Dou, S.; Colby, R. H.; Runt, J. Molecular Mobility and Li^+ Conduction in Polyester Copolymer Ionomers Based on Poly(ethylene oxide). *J. Chem. Phys.* **2009,** *130*, 064907.

50. Nakamura, K.; Saiwaki, T.; Fukao, K. Dielectric Relaxation Behavior of Polymerized Ionic Liquid. *Macromolecules* **2010,** *43*, 6092-6098.

51. Love, S. A.; Popov, E.; Rybacki, K.; Hu, X.; Salas-de la Cruz, D. Facile Treatment to Fine-Tune Cellulose Crystals in Cellulose-Silk Biocomposites through Hydrogen Peroxide. *Intl. J. Biological Macromolecules* **2020,** *147*, 569-575.

52. Stanton, J.; Xue, Y.; Pandher, P.; Malek, L.; Crown, T.; Hu, X., Salas-de la Cruz, D. Impact of Ionic Liquid Type on the Structure, Morphology and Properties of Silk-Cellulose Biocomposite Materials. *Intl. J. Biological Macromolecules* **2018,** *108*, 333-341.

53. Choi, U. H.; Ye, Y.; Salas-de la Cruz, D.; Liu, W.; Winey, K. I.; Elabd, Y. A.; Runt, J.; Colby, R. H. Dielectric and Viscoelastic Responses of Imidazolium-Based Ionomers with Different Counterions and Side Chain Lengths. *Macromolecules* **2014,** *47*, 777-790.

54. Salas-de la Cruz, D.; Green, M. D.; Ye, Y.; Elabd, Y. A.; Long, T. E.; Winey, K. I. Correlating Backbone-to-Backbone Distance to Ionic Conductivity in Amorphous Polymerized Ionic Liquids. *J. Polym. Sci. B Polym. Phys.* **2012,** *50*, 338-346.

55. Liu, H.; Paddison, S. J. Direct Comparison of Atomistic Molecular Dynamics Simulations and X-ray Scattering of Polymerized Ionic Liquids. *ACS Macro. Lett.* **2016,** *5*, 537-543.

56. Paren, B. A.; Raghunathan, R.; Knudsen, I. J.; Freyer, J. L.; Campos, L. M.; Winey, K. I. Impact of Building Block Structure on Ion Transport in Cyclopropenium-Based Polymerized Ionic Liquids. *Polym. Chem.* **2019,** *10*, 2832-2839.

57. Griffin, P. J.; Freyer, J. L.; Han, N.; Geller, N.; Yin, X.; Gheewala, C. D.; Lambert, T. H.; Campos, L. M.; Winey, K. I. Ion Transport in Cyclopropenium-Based Polymerized Ionic Liquids. *Macromolecules* **2018,** *51*, 1681-1687.

58. Blessing, B.; Trout, C.; Morales, A.; Rybacki, K.; Love, S. A.; Lamoureux, G.; O'Malley, S. M.; Hu, X.; Salas-de la Cruz, D. Morphology and Ionic Conductivity Relationship in Silk/Cellulose Biocomposites. *Polym. Int.* **2019,** *68*, 1580-1590.

TABLE OF CONTENTS GRAPHIC